Research Article

Regeneration and Reusability of Bleaching Earth as a Sustainable Material for Tartrazine Yellow (E102) Removal: Insights into Kinetic Mechanisms

Chaida Butumap Ngolong Ngwethe[1], Gervais Kounou Ndongo[2, 3], Donald Raoul Tchuifon Tchuifon[1*], Cyrille Ghislain Fotsop[4], Dave Sanchez Mouafo Dongmo[1], Urselin Roland Noumsi Foko[1], Lynda Nathalie Nkom Soue[1], Melea Charles Kede[1]

[1]Department of Process Engineering, Laboratory of Energy, Materials, Modeling and Method, National Higher Polytechnic School of Douala, University of Douala, P.O. Box 2701 Douala, Cameroon
[2]Department of Fondamental Sciences, University Institute of Wood Technology of Mbalmayo, University of Yaounde I, P.O. Box 306, Mbalmayo Cameroon
[3]Applied Physical and Analytical Chemistry Laboratry, Department of Inorganic Chemistry, Faculty of sciences, University of Yaoundé I, P.O. Box 812, Yaounde, Cameroon
[4]Institute of Chemistry, Faculty of Process and Systems Engineering, Universität Platz 2, 39106 Magdeburg, Germany
Email: tchuifondonald@yahoo.fr

Abstract: Anionic dyes, like tartrazine, have harmful effects on aquatic life and humans and therefore, their elimination from industrial effluents needs to be taken very seriously. The elimination of tartrazine yellow from wastewater resulted in the application of adsorption as an economical and effective treatment approach. The use of regenerated bleaching earth and regenerated bleaching earth modified with urea as adsorbents for tartrazine yellow from simulated wastewater served as the foundation for this study. The sorption process was run in batch mode with different process parameters. The Fourier transform infrared spectrophotometry (FTIR) and X-ray diffraction analyses of the adsorptive material demonstrated the existence of surface functional groups while scanning electron microscopy revealed a porous structure. At a pH of 3, with an adsorbent dosage of 50 mg and a dye concentration of 50 mg/L, the highest dye uptake was achieved with an adsorption efficiency of 48%. The models that best matched the kinetics were the pseudo-first-order, pseudo-second-order and Elovich ($R^2 > 0.95$) models. The dye fixation process took 140 minutes to reach adsorption equilibrium. The outcomes of the sorption study demonstrated competition between chemisorption and physisorption, and that bleaching earth can be successfully regenerated, and used as an efficient sorbent for eliminating tartrazine yellow in an aqueous solution.

Keywords: bleaching earth, regeneration, adsorption, tartrazine yellow

1. Introduction

Owing to their large specific surface areas and high adsorption capacities, MOFs (Metal organic frameworks) and activated carbons are commonly utilized in the adsorption process.[1,2] Nevertheless, this method is rather costly. As a result, using novel adsorbents made of abundantly available natural materials like clays, which are naturally occurring

aluminosilicates was given more importance.[3] Clay materials often possess limited adsorption capacities and exist in a range of natural forms. As such, they are not widely used for the sorption of pollutants. They undergo modifications like chemical or thermal activation to increase their adsorption capabilities.[4]

While natural clays hold promise as low-cost adsorbents, their inherent limitations in adsorption capacity and selectivity hinder their widespread application. This study addresses this challenge by investigating the regeneration and urea modification of bleaching earth, a waste product from the edible oil industry, to improve its capacity for tartrazine dye adsorption.

This research focuses on enhancing the adsorption performance of bleaching earth through regeneration and urea modification. Regeneration allows for the reuse of waste material, promoting sustainability. Urea modification, which will be further explained later, is specifically chosen to target an improvement in either the adsorption capacity (the total amount of dye the material can hold). By understanding the impact of regeneration and urea modification, we can develop a more efficient and cost-effective method for dye removal from wastewater. Bleaching earth, commonly known as sulfuric acid-activated clay is extensively used in the food processing industry to decolorize edible oils. This material is very effective at removing unwanted materials from oil, including soap residues, heavy metal traces, and colors like β- and α-carotene.[5-6] Bleaching earth (BE@oil) is a detritus that is produced when the sulfuric acid-activated clay material used to decolorize oil loses its ability to adsorb any further. This solid material is considered as waste and dumped untreated into the environment. For this reason, much research is being diverted to the regeneration and reuse of this clay waste to minimize the danger of pollution.[7-10]

Dyes are frequently used in the textile, rubber, paper, plastic, cosmetic, and other sectors to colour various products. Residual dyes in effluents are nearly always the primary waste product in these industries. Due to their chemical structures, dyes are resistant to fading when exposed to light, water, and various chemicals, making them challenging to decolorize once discharged into the aquatic environment.[11-12] A multitude of organic dyes are hazardous and may affect aquatic life in addition to the food chain. The anionic azo dye known as tartrazine (C.I. Acid Yellow 23, AY23) is present in a vast number of foods and pharmaceuticals. Asthma, urticaria, and angioedema have all been linked to the dye. [13-14]

Edible oil refineries produce significant quantities of waste in the form of used bleaching earth, which represents a major environmental challenge due to the complexity and cost of their disposal. Although the exact quantity of used bleaching earth generated annually is unknown, the enormous volume of refined oil indicates a significant waste stream. For example, processing the growing global consumption of palm oil would require approximately 1.5 million tonnes of land in 2021[1], which is only a fraction of the total. This number highlights the potential scale of the waste problem. In addition, the management of this solid waste is proving increasingly difficult: using bleaching earth, considered hazardous waste due to its properties, is difficult and costly to dispose of, with risks of soil contamination and the air. The volumes produced also pose a storage and treatment problem, making the management of this waste increasingly problematic.

The least squares method and the linear regression approach have been used to find the model parameters and identify the best-fitting models respectively.[15-17] Once a linear regression has been plotted, the parameters are determined using the slope and line intercepts. The adsorption kinetic and isotherm model that best fits the adsorption data is selected based on the correlation coefficient (R^2).[18] A major drawback of linear regression is that its error distribution is not fixed.[19-20] Furthermore, in the case of kinetics and isotherms with more than two parameters, linear regression is unsuitable to ascertain the value of unknown parameters using the graphical approach.[21] More recently, non-linear regression has been used in adsorption research in place of linear regression when developing models in conjunction with error analysis.[17] For non-linear analysis, a variety of error analysis methods, such as residual root mean square error (RMSE),[22] non-linear chi-square test error function (χ^2),[23] and coefficient of determination (R^2)[24] are applied to determine the suitably of kinetic and isotherm models.

In this work, a food-grade dye called tartrazine yellow in an aqueous solution was adsorbed onto regenerated and modified bleaching earth. The optimization of sorption kinetics and parameters was investigated in batch mode.

2. Experimental methods

The clay known as bleaching earth is primarily composed of three minerals: attapulgite (a fibrous alumino-magnesian clay typically consisting of fibres of the order of 1 to 3 microns long), stévensite-kerolite (a mineral composed of magnesium silicates), and bentonite (a gray-white mineral composed of montmorillonite, i.e. magnesium aluminum silicate and crystalline silica in a lesser proportion). Its characteristics are listed in Table 1 below.

Table 1. Characteristic of bleaching earth (BE)

Physical state	Solid, powder
Color	Beige
Melting point	> 450 °C; EU A 1 method
Decomposition temperature	> 450 °C
pH	5-6.5 (10% suspended solid in water)
Solubility in water	< 0.9 mg/L at 20 °C, EU A 1 method
Relative density	2.6 g/cm^3 at 20 °C
Average particle diameter	20-40 μm

In its pure state, tartrazine is a yellow powder with a golden hue that dissolves in water when exposed to sunshine. Despite being restricted by several standardizing authorities, it is widely utilized in many industries, most notably the food, cosmetics, and 3D printing industries. Its characteristics are listed in Table 2.

Table 2. Characteristics of E102 dye, tartrazine yellow[25]

Nomenclature	Tartrazine yellow
Chemical formula	$C_{16}H_9N_4Na_3O_9S_2$
structure	
solubility	200 g/L at 25 °C
Molecular weight	543.36 g/mol
IUPAC Name	Trisodium; 5-oxo-1-(4-sulfonatophenyl)-4-[(4-sulfonatophenyl)diazenyl]-4-Hpyrazole-3-carboxylate
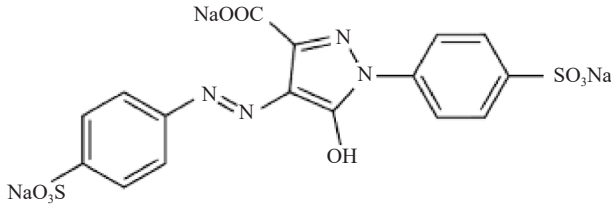
2.1 Preparation of regenerated bleaching earth (RBE)

The bleaching earth (BE@oil) used in this work comes from a palm kernel oil refining factory located in the city of Douala, Wouri department, Littoral region of Cameroon and it was subjected to physicochemical treatment to yield regenerated bleaching earth. The SOXHLET device was initially set up, and BE@oil was used as the primary reagent

and hexane as the solvent in a de-oiling procedure for the material. Next, a BE@oil-H_2SO_4 mixture was made and was agitated for 4 hours at 150 rpm. The sulfuric acid solution of concentration 1 M made up 20% of the combination. After stirring, the solid residue was thoroughly washed with distilled water to get rid of any remaining acid, and it was then dried for 24 hours at 105 °C. A portion of this material was calcined for three hours at 550 °C, yielding a product known as RBE.

In order to modify the material with urea, 200 mL of distilled water was put into a 500 mL Erlenmeyer flask along with 20 g of BE and 20 g of urea. The mixture was agitated at 200 rpm for 24 h, filtered and the residue dried for 12 h at 105 °C, before calcining at 550 °C to produce RBE@N. The various materials so obtained are crushed, sieved through sieves with a diameter of 100 μm, and then kept in a desiccator for further use. A simple description of bleaching oil regeneration is shown in Figure 1.
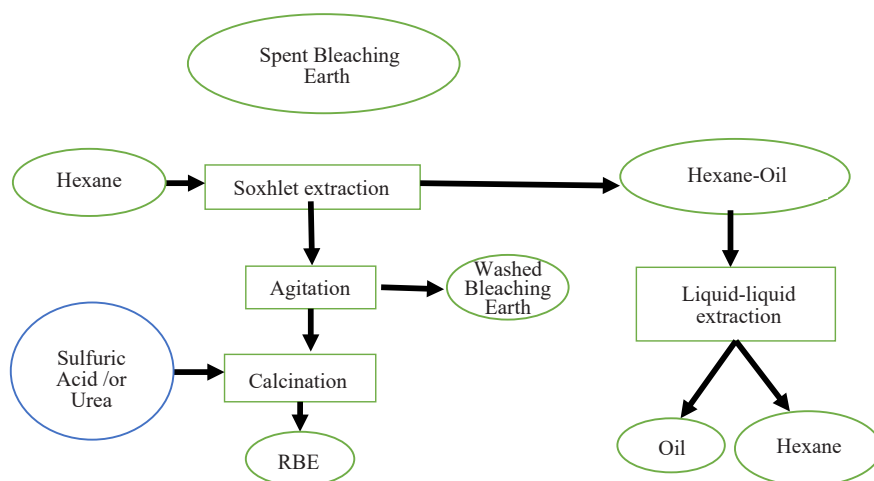
Figure 1. Oil recovery and regeneration of used bleaching earth processes

2.2 *Materials analysis techniques*

2.2.1 *Determination of acidity of materials*

For each material (BE, RBE, and RBE@N), 1.25 g of it was put into 25 mL of distilled water. The mixture was agitated for 30 minutes and filtered. The filtrate was titrated against 0.1 N NaOH solution using the following formula.

$$(HCl) \% \ Acidity = 0.78 x N x V_{NaOH}$$

where N is normality the titrant solution and V_{NaOH} is the burette reading.

2.2.2 *pH at the point of zero charge (pH$_{PZC}$) determination*

The pH at which the adsorbent's surface is free of both positive and negative charges is known as the pH$_{PZC}$. Both the pH of the solution and the pH$_{PZC}$ of the adsorbent's surface play a significant role in the solute's ability to bind to a solid surface. 0.1 g of each material was added to a series of flasks containing 50 mL of 0.01 M NaCl solution with pH values ranging from 2 to 12, and the mixture was agitated for 48 hours. The pH filtrates were measured after filtering. The point at which the line graph of $\Delta pH = f(pH_{intitial})$ intersects with the adsorbent is its pH$_{PZC}$.

2.2.3 *XRD, FTIR, SEM-EDX mapping analysis*

Undoubtedly, the solid's heat treatment caused changes to the material's structure. Several methods, such as scanning electron microscopy coupled to Energy dispersive X-ray spectroscopy, Fourier transform infrared

spectrophotometry (FTIR), and X-ray diffraction (XRD) have been utilized to study the properties of the prepared materials. A Genesis FTIRTM spectrometer (Bruker Optik GmbH, Rudolf-Plank-Str. 27, 76275 Ettlingen, Germany) (ATI Mattson) fitted with a DTGS (Deuterated Tri Glycine Sulfate) detector in the transmission mode from 200 to 4,000 cm^{-1} after 20 scans was used to record Fourier-transform infrared (FTIR) spectra.

Ex-situ XRD data was obtained using a DECTRIS® MYTHEN 1K detector (DECTRIS, Baden-Daettwil, Switzerland) in transmission geometry with Cu Kα1 radiation (λ = 1.54056 Å; Gemonochromator; flat samples) on an STOE Stadi-p powder X-ray diffractometer (STOE & Cie GmbH, Darmstadt, Germany). Using a Magellan 400 L scanning electron microscope, field-emission scanning electron microscopy combined with energy-dispersive X-ray microanalysis (FE-SEM/EDX) was used to study the surface morphological features and elemental compositions of the materials.

2.3 Sorption experiments

Tartrazine yellow was used without any additional purification. To make a stock solution, the necessary quantity of tartrazine was dissolved in distilled water to yield a 1,000 mg/L concentration. A SECOMAM visible spectrophotometer was used to measure the absorbance at λ_{max} = 428 nm in order to generate a calibration curve. Multiple standard solutions were created from the stock solution in the concentration range of 20 to 100 mg/L. Using decimolar nitric acid and sodium hydroxide, the pH of the solutions were adjusted during the tests. In 100 mL conical flasks, batch adsorption was performed by combining 15 mL of an aqueous dye solution with a preweighed quantity of the adsorbent. Conical flasks were placed on a magnetic stirrer and stirred at a steady speed of 150 rpm for a predetermined time. Operational parameters, including pH, agitation time, and adsorbent dosage, were varied for optimization purposes. At the end of each adsorption process, the mixture was filtered, and a spectrophotometer (SECOMAM, model S 500) was used to measure the filtrate's residual concentration. Equation 1 was used to compute the amount of dye adsorbed (mg/g) while the dye removal efficiency ($\%_{ads}$) was ascertained using the formulae in Equation (2) below,

$$Q_e = \left(C_i - C_f\right)V/m \tag{1}$$

$$\%_{ads} = \left(C_i - C_f\right)\times 100/C_i \tag{2}$$

Where Q_e is the amount of dye adsorbed from the solution, V is the volume of the adsorbate, C_i is the initial concentration of tartrazine yellow, C_f is the concentration after adsorption, and m is the mass in grams of the adsorbent.

2.3.1 Effect of initial pH of dye solution

In the pH range of 3.0 to 11.0, 100 mg of the adsorbent was agitated in a 15 mL aqueous solution containing 50 mg/L of tartrazine to ascertain the influence of pH. HNO$_3$ or NaOH was used in order to adjust the pH. The solution was quickly filtered after an hour, and a spectrophotometer was used to measure the residual concentration. Using equation (1), the amount of tartrazine adsorbed (Q_e) was determined.

2.3.2 Effect of contact time

By agitating 100 mg of ground adsorbent in a 15 mL solution of tartrazine with an initial concentration of 50 mg/L at varying time intervals, the impact of agitation time on the adsorption process was assessed. After each respective time of contact, the spectrophotometer was used to measure the residual concentration after the solution had been quickly filtered. Using equation (2), the percentage elimination ($\%_{ads}$) of tartrazine was determined.

2.3.3 Effect of adsorbent dosage

In this series of tests, a 15 mL solution of tartrazine with an initial concentration of 50 mg/L was used to agitate a range of adsorbent masses, from 25 to 175 mg.

2.4 Adsorption kinetics

Several kinetics models were tested to determine the best fitting model for the adsorption of tartrazine onto the biosorbents.

The pseudo-first order equation is generally expressed as in equation 3[26]

$$Q_t = Q_e \left[1 - \exp\left(-K_1 t \right) \right] \tag{3}$$

With K_1: adsorption rate constant (g/mg·min); Q_e: quantity adsorbed at equilibrium (mg/g) and Q_t: quantity adsorbed at time t (mg/g).

The pseudo-second order chemisorption kinetic equation is given by equation 4[27]

$$Q_t = \frac{Q_e^2 K_2 t}{1 + Q_e K_2 t} \tag{4}$$

With K_2: pseudo-second order adsorption rate constant (g/mg·min); Q_e: quantity adsorbed at equilibrium (mg/g) and Q_t: quantity adsorbed at time t (mg/g).

The Elovich equation is generally expressed by equation 5[28]

$$\frac{dq_t}{dt} = \alpha e^{(-\beta q_t)} \tag{5}$$

To simplify the Elovich equation, Chien and Clayton in 1980 assumed that $\alpha\beta t \gg 1$ and applying the initial conditions $Q_t = 0$ to $t = 0$ the equation 5 becomes:

$$Q_t = \frac{\ln(\alpha\beta)}{\beta} + \frac{\ln t}{\beta} \tag{6}$$

With α: the initial adsorption rate (g/mg·min); β: desorption rate constant(g/mg·min) and Q_t: amount adsorbed at time t (mg/g).

The intraparticle diffusion model is expressed as in equation 7[29]

$$Q_t = K_{id} t^{1/2} + C \tag{7}$$

With K_{id}: Weber intraparticle diffusion rate constant in (mg/g·min$^{1/2}$); Q_t: amount adsorbed at time t (mg/g); C: value of the thickness of the boundary layer.

2.5 Error functions

In this study, the curve was fitted using non-linear regression and the Microsoft Excel Solver feature from Excel 2019. The coefficient of determination (R^2), residual root mean square error (RMSE), and Chi-square test (χ^2) were used to evaluate which model best fits the experimental data. According to[15,30-31] the error function expressions are as follows.

$$\chi^2 = \sum_{i=1}^{N} \frac{\left(Q_{e,\,exp} - Q_{e,\,cal} \right)^2}{Q_{e,cal}} \tag{8}$$

$$RMSE = \sqrt{\frac{1}{N-2}\sum_{i=1}^{N}\left(Q_{e,\,\exp} - Q_{e,\,cal}\right)^2} \tag{9}$$

$$R^2 = \frac{\sum_{i=1}^{N}\left(Q_{e,\,cal} - Q_{e\exp}\right)^2}{\sum_{i=1}^{N}\left(Q_{e,\,cal} - Q_{e\exp}\right)^2 + \left(Q_{e,\,cal} - Q_{e\exp}\right)^2} \tag{10}$$

Where $Q_{e,exp}$ and $Q_{e,cal}$ (mg/g) are the equilibrium capacity of adsorption obtained experiment ally and by calculations from the models, respectively and N is the number of data points.

3. Results and discussion

3.1 *Characterization of materials*

3.1.1 *Determination of pH and pH at the point of zero charge of materials*

The pH value at which there is no net charge on the surface of the adsorbents is known as the pH_{PZC} or pH at the point of zero charges. In adsorption phenomena, this value is crucial, particularly when electrostatic forces play a role in the mechanisms. By plotting ΔpH ($pH_{final} - pH_{initial}$) against pHinitial, we were able to calculate the pH of zero charge (pH_{PZC}). The outcomes are displayed in Figure 2.
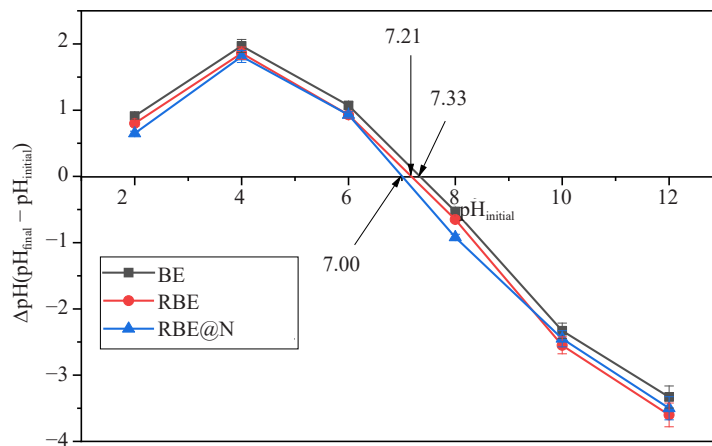
Figure 2. pH at the point of zero charges of the materials

The isoelectric and pH point values of different materials are shown in Table 3.

The uptake of H^+ ions added to the solution by the surfaces of the solids can be used to explain the first portion of the three curves in Figure 2, where the $pH_{final} - pH_{initial} > 0$. This curve shows that the final pH of the solution increases with an increase in the initial pH. In the second section, where $pH_{final} - pH_{initial} = 0$, all H^+ ions added to the solution are actually absorbed by the solid's surface until the sites are saturated, at which point the solution's pH_{final} rises. This section relates to the OH^- ion surface saturation, at which point all of the added OH^- ions stay in solution.[32] The results presented in Table 3 suggest that the bentonite treatment did not significantly alter the adsorbent's acidity, hence facilitating improved dye adsorption in the medium. Negative charges accumulate on the surfaces of the adsorbents for solution pH below pH_{PZC}. Tatrazine yellow is thus favourable for adsorption onto these materials due to a notably strong electrostatic affinity between the OH-ions on the adsorbents' surface and the dye's form. The adsorbents' positively

charged surfaces, on the other hand, are more likely to reject the dye's cations at pH values higher than pH_{PZC}.

Materials	BE	RBE	RBE@N
pH_{Pzc}	7.33	7.21	7.00
pH	6.04	6.02	6.05

3.1.2 *Fourier-transform infrared spectroscopy*

Figure 3 shows the infrared spectra of the different materials. All materials exhibit a strong band centered at 1,001 cm^{-1} and ranging from 1,200 cm^{-1} to 900 cm^{-1}, which is consistent with the Si-O (Quartz) bond's valence vibrations, according to spectroscopic investigation.[33] Stretching vibrations of Si-O-Al bonds (Kaolinite) and hydroxy groups perpendicular to the surface (translational OH) are responsible for the bands between 795 cm^{-1} and 748 cm^{-1}.[34-35] The illite's vibrations may be the cause of a band that is present between 690 and 750 cm^{-1}.[36] Nevertheless, other peaks that indicate the existence of additional substances were detected in the spectrum of waste-bleaching earth (BE@oil) alone. These peaks are as follows: The elongation of nitro compounds (N-O group) is represented by the existence of a band at 1,500 cm^{-1}. The band, which stretches between 1,700 cm^{-1} and 1,600 cm^{-1}, is caused by the valence vibrations of the OH group of the water adsorbed between the layers. The presence of organic molecules confirms that the bands between 3,000 and 2,840 cm^{-1} are typical of the C-H elongation of alkanes.
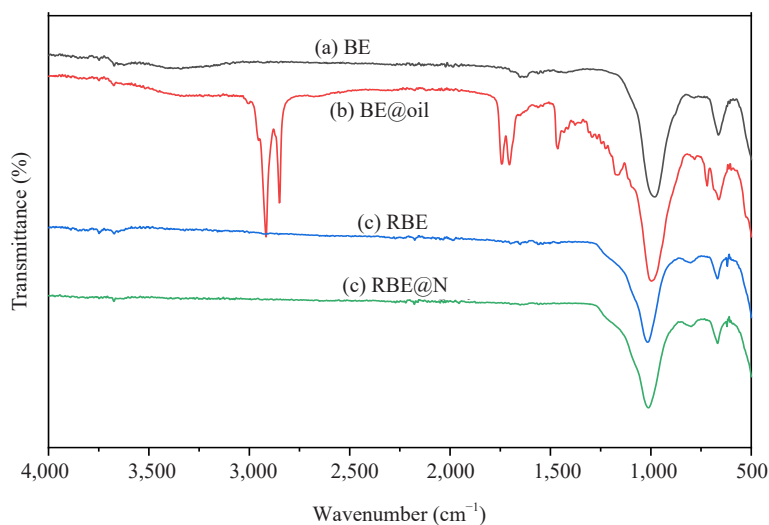
Figure 3. FTIR of different materials (a) BE, (b) BE@oil, (c) RBE and (d) RBE@N

3.1.3 *Scanning electron microscopy*

The images of the surface morphologies of the materials obtained from SEM analysis are presented in Figure 4.

The tetrahedral (T) and octahedral (O) layers of oxygen atoms stack to form a layered structure of this clay, as observed under a scanning electron microscope of the BE. It was also observed that in contrast to other clays, such as BE@oil that has been washed with sulfuric acid and BE@oil, which has been used to decolorize vegetable oils while also taking modifying agents into account, the color of BE is white.[37] The BE@oil image demonstrates how the clay that resulted from the discoloration phenomena is now dark or perhaps black in appearance rather than white. This can

be the result of contaminants removed from crude palm oil during the refining process. The original structure is still visible in this micrograph, but it appears to have less developed porosity than the BE. It's possible that this is because of substances that were left behind after it was used to decolorize crude palm oil and that washing was unable to remove these substances. It can also be seen that the clay-like morphology appears to be different for RBE compared to raw-bleaching earth. It appears to have higher porosity than any other material while retaining the white hue that is specific to its clay. Regarding RBE@N, it has a layered structure that differs from the raw bleaching earth-based clay. The modification of the bleaching earth with urea might have had an impact on how the oxygen tetrahedral (T) and octahedral (O) layers are stacked, which would have allowed for an increase in pores on the material's surface. Its original clay's unique white tint, however, is still present and unaltered.
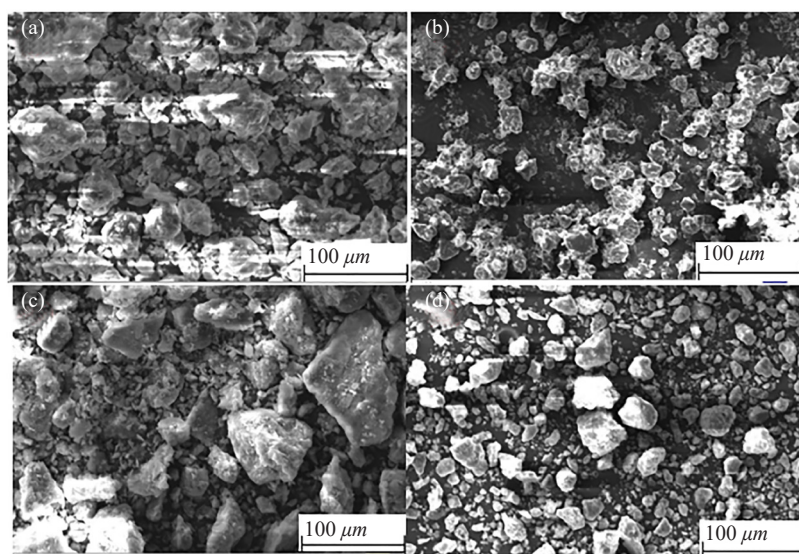
Figure 4. SEM image of (a) BE, (b) BE@oil, (c) RBE et (d) RBE@N

3.1.4 *Energy dispersive X-ray spectroscopy (EDX)*

This technique was used to determine the elemental composition of the various materials used in this study. The outcomes of the SEM-EDX analysis are shown in the Figure 5.

The chemical composition of the raw BE material (Figure 5a) was determined qualitatively by EDX microanalysis to yield percentages of oxygen (O), magnesium (Mg), aluminum (Al), and silicon (Si) that are, respectively, 47.8%, 18.8%, 1.4%, and 32%. After refinement, EDX analysis shows the presence of two more elements: carbon and phosphorus. On the one hand, there is a decrease in the percentage composition of some elements (silicon, magnesium, and oxygen), which is followed by an increase in the mass percentage of Al. Raw bleaching earth conserved these chemical components, which could be a result of the presence of oil contaminants (Figure 5b).

The results obtained (Figure 5c) show that the elemental makeup of the RBE is the same as that of the BE; nevertheless, we observe that the element Na is present. The montmorillonite compound $((Al_{1.67}Mg_{0.33})Si_4O_{10}(OH)_2Na_{0.33})$ is characterized by the presence of the element Na. In contrast to the original modified clay, the RBE@N exhibits the presence of urea-specific atoms such as carbon and nitrogen (Figure 5d). The increase in Si content in the regenerated bleaching earth (RBE) is due to the combination of selective removal of non-siliceous impurities and decomposition of aluminosilicates during the regeneration process.[2]
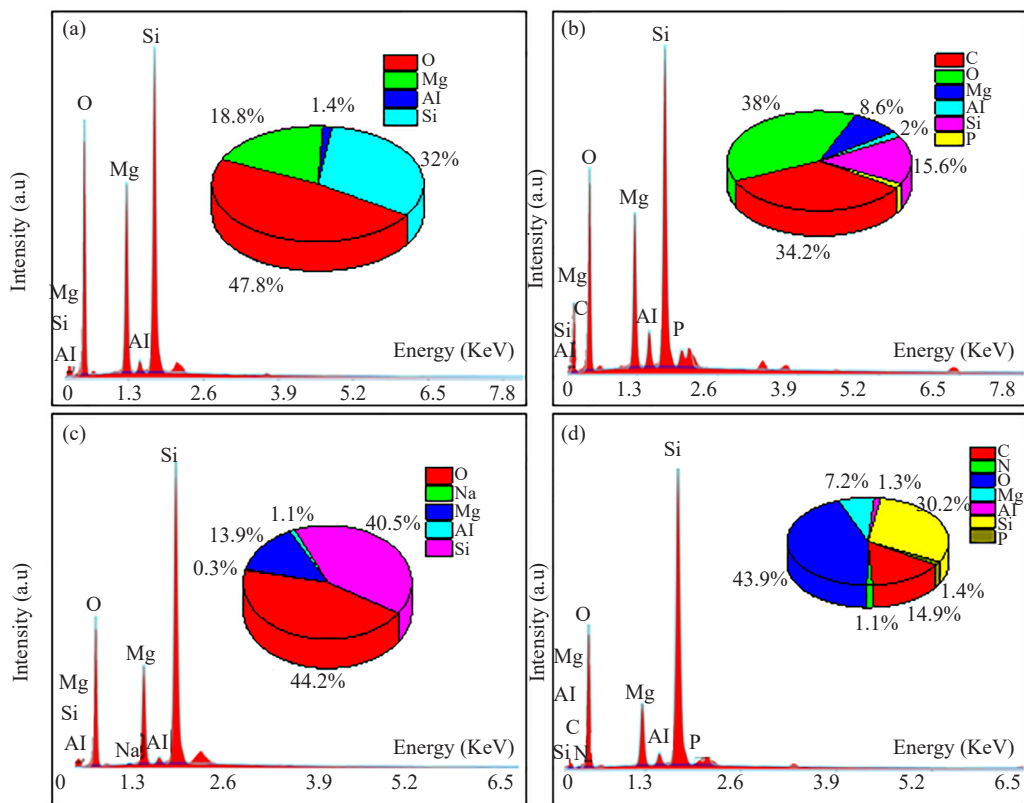
Figure 5. EDX elemental compositions of (a) BE, (b) BE@oil, (c) RBE and (d) RBE@N

3.1.5 *X-ray diffraction (XRD)*

Using X-ray diffraction analysis, we were able to identify the mineralogical phases that make up the mineral powders under investigation.
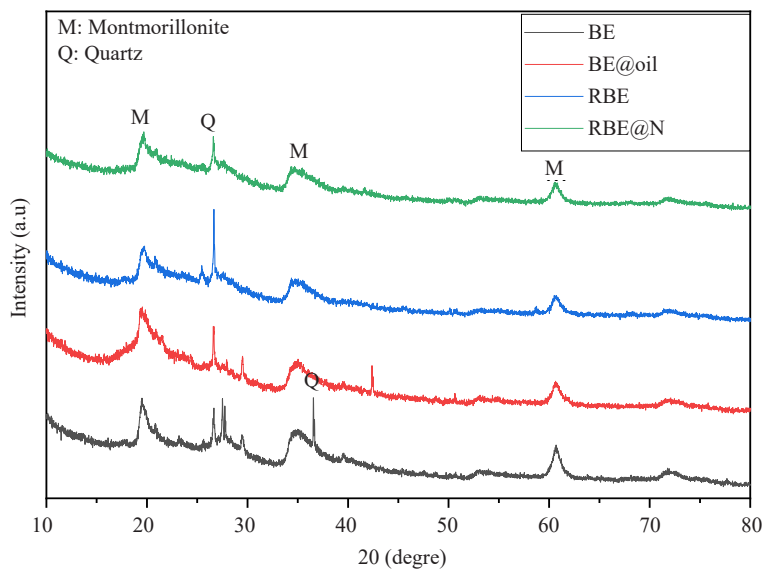
Figure 6. XRD of the different materials

Figure 6 shows the X-ray diffractograms of RBE, RBE@N, BE and BE@oil materials. The results reveal that the spectra do not significantly differ from one another. The primary crystallographic structure of the clay is unaffected by the adsorption of colours (such β carotene, chlorophyll, etc.) from the treated oils or the various bleaching earth treatment processes. The bentonite's diffractogram reveals that silica (SiO_2) predominates in quartz crystals, as evidenced by a Montmorillonite and quartz. The diffractogram as a whole is defined as follows:

-20.89°, 20.73; 37.5°; and 50.78°, which characterize quartz (Q);

-19.94°, 35.8°, and 61.7°, which characterize montmorillonite (M).[38]

According to Komadel et al.[39], the diffractograms for the clays BE, BE@oil, RBE, and RBE@N indicate that the first peak at $2\theta = 19.4°$, which corresponds to montmorillonite in the BE, is attenuated in the RBE. This suggests that during the acid treatment, the protons from the acid replace the interfoliar cations, leading to the dissolution of the octahedral cations (Al^{3+}, Mg^{2+}, Fe^{2+}, and Fe^{3+}). Additionally, Fermandes et al.[40] showed that contaminants are reduced by acid treatment. This result leads us to the conclusion that the bleaching earth's original structure remains unchanged following the chemical treatment of the regenerated material.

-Quartz's second peak, $2\theta = 20.73°$, is visible on all materials but is more prominent on the RBE. As a result, we would anticipate that RBE's adsorbent power would be higher than BE's because silica is a substance whose specific surface area increases with temperature.[41]

-The BE spectrum is the only one with the third peak, $2\theta = 38°$, representing quartz; the other spectra do not have it. We may comprehend that there would have been more movement or a chemical reaction between the components of quartz and the contaminants in the raw palm oil when this clay was used in the decolorization of oil (BE@oil).

3.2 *Adsorption studies*

The mass of the adsorbent material, the pH of the pollutant solution, and the contact time were all varied to emphasize the impact of key parameters that are likely to affect the adsorption process. These parameters are related to the adsorbate's nature (size, polarity, solubility, presence of functional groups) as well as the adsorbent's physical characteristics (porous structure, type of surface functional groups).

3.2.1 *Influence du pH*

Different solutions of the dye (50 mg/L), adjusted separately to pH values between values 3 and 11 were brought into contact with the adsorbent at a dosage of 50 mg, to study the effect of pH on the adsorption of the dye on the two clay materials. Figure 7 presents the results obtained.
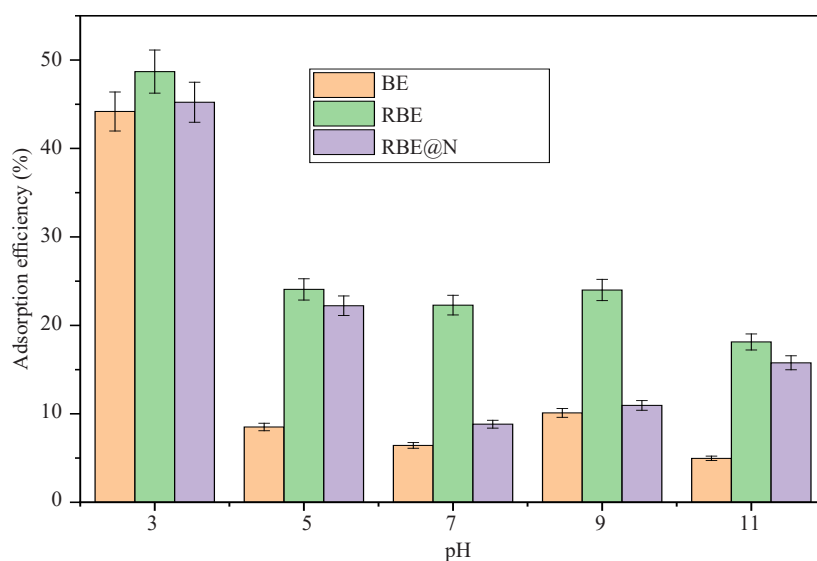
Figure 7. Influence of pH on adsorption

The best elimination rates for the pollutant E102 are often achieved at an acidic pH (pH 3), as shown in Figure 7. These rates are 48% for RBE, 45% for RBE@N, and 44% for BE. The adsorption of the dye onto the various materials decreased by half for the modified materials and by five times for BE (4% for RBE, 22% RBE@N, and 8% BE) when the pH rose above 5.

The degree of dissociation of various compounds in solution at various pH values and the surface charge of the adsorbents can both be used to explain these tendencies.[42]

This is because as the pH of the adsorbate increases, the positively charged sites on the adsorbent get decreased (with a consequent increase in negative charges on the adsorbent) thereby causing less attraction of the anionic dyes for the surface of the adsorbent. This condition leads to electrostatic repulsion because it does not support the uptake of anionic dyes from the system.[43] A decrease in sorption of dyes is observed at high pH, this is because hydroxide (OH$^-$) ions compete effectively for the active site on the adsorbent with the anionic dye. The enhanced electrostatic force of attraction exists between the the three adsorbent and anionic dyes at pH < 4 thereby increasing the removal of the dyes. At lower adsorbate pH, the adsorbent surface gets protonated, resulting in increased dye adsorption due to electrostatic attraction. A similar result was recorded in the sorption of tartrazine onto sawdust biosorbent.[44]

3.2.2 Influence of contact time

Determining the point at which equilibrium is reached requires an understanding of how contact time affects dye uptake into any substance. Figure 8 illustrates the influence of contact time on the uptake of tartrazine onto BE, RBE, and RBE@N. It is evident that there was no discernible increase in the sorption rate following the initial rapid rate of dye fixation from the solution, which was followed by a gradual decrease until equilibrium was reached.

The initial phases of the adsorption process are attributed to the many vacant surface-active sites on the adsorbent, which saturate with time, indicating the achievement of adsorption equilibrium.[45] It was noted that all three adsorbents had the same equilibrium periods (140 min). For BE, RBE, and RBE@N, equilibrium adsorption capacities for the tartrazine molecules are 1.40, 2.43, and 2.30 mg/g at 140 minutes, respectively.
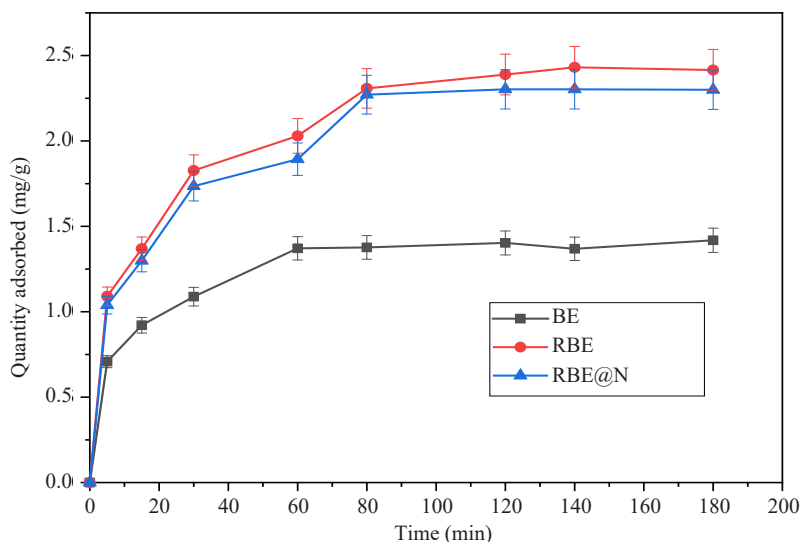
Figure 8. Influence of contact time on the adsorption of E102

3.2.3 Influence of the mass of the adsorbent

As an essential factor in adsorption research, the adsorbent dose establishes the adsorbent's capability for a specific starting dye concentration. Figure 9 illustrates how dosage affects tartrazine's ability to bind to BE, RBE, and RBE@N. With an increase in material dose, the dye's ability to be absorbed by BE, RBE, and RBE@N is reduced. The adsorption

capacity of tartrazine decreased from 2.66 to 0.16 mg/g, 6.27 to 0.97 mg/g, and 3.60 to 0.29 mg/g for BE, RBE, and RBE@N, respectively when the adsorbent dosage was increased from 25 to 175 mg.

The decrease in the adsorption capacities of BE, RBE, and RBE@N is due to aggregation/overlapping of the active adsorption sites at higher doses of the materials.[46] Consequently, more dye loading is achieved at lower adsorbent dosages due to more effective utilization of the active sites of BE, RBE, and RBE@N. Remember that the concentration of tartrazine does not change with an increase in the material dosage. This encourages less loading on the material's specifically active sites, which reduces site usage.[47]

To guarantee the best possible use of the adsorption sites, we chose 50 mg of each adsorbent for the adsorption investigation. Other researchers have also observed a similar pattern in the removal of dyes[48,49] and heavy metals[50,51] from contaminated water.
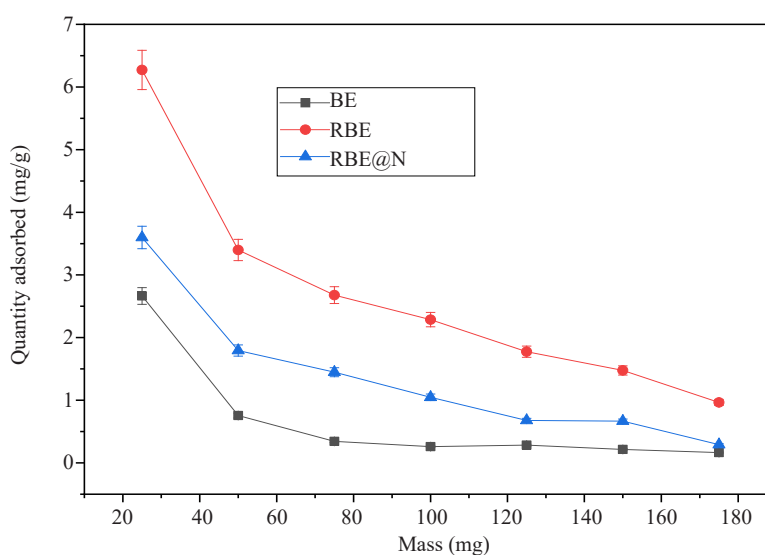
Figure 9. Influence of material doasage on E102 adsorption

3.3 *Kinetic analysis*

For the purpose of describing the adsorption process mechanism and rate, kinetics offers useful information. The mechanism of adsorption was examined in this work using pseudo-first-order, pseudo-second-order, Elovich, and intraparticle diffusion models. Table 4 presents the kinetic rate constants, while Figure 10 shows the non-linear kinetic plots.

All three of the adsorbents have coefficients of determination (R^2) more than 0.95 for the pseudo-first-order, pseudo-second-order, and Elovich models. The computed values of $Q_{e(cal)}$ for the pseudo-first and pseudo-second-order models of tartrazine dye showed almost the same values as the experimental value of equilibrium sorption capacity, $Q_e(exp)$. The results of the Chi-square test (χ^2) indicated that the Elovich, pseudo-first-order, and pseudo-second-order models fit the experimental data the best. According to the results of the pseudo-second-order and Elovich models,[51] this good fit suggests that both internal and external mass transfer mechanisms were important factors in the uptake of tartrazine dye on BE, RBE, and RBE@N. The results of the pseudo first-order model, indicate a physisorption process for the dye uptake, from which we can conclude that there is strong evidence that physisorption and chemisorption participate in the adsorption process of tartrazine on these three adsorbent materials.

The intraparticle diffusion model assumes that the dye molecules diffuse inward into the porous adsorbent. The values of the R^2 recorded for the uptake of the dye onto BE, RBE and RBE@N were low ($0.732 < R^2 < 0.877$), indicating that the intraparticle diffusion is not the dominant mechanism for the removal of the dye molecules by adsorption onto BE, RBE and RBE@N. Besides, the intraparticle diffusion model had intercept values indicating the involvement of the surface sorption process.[52]
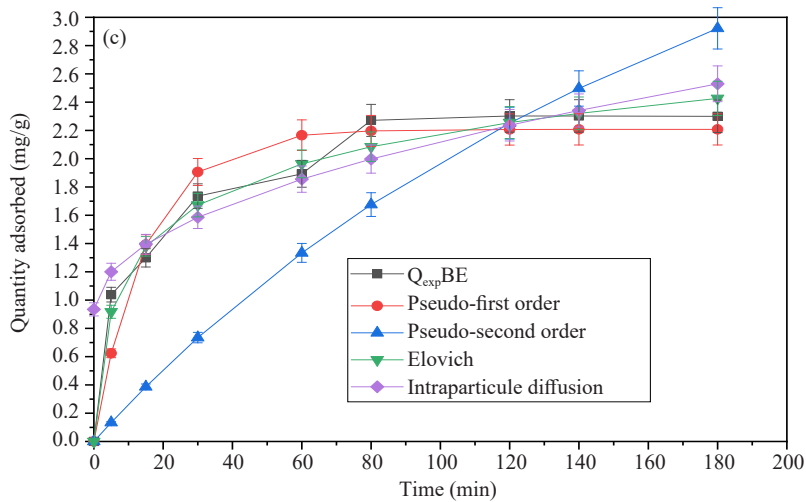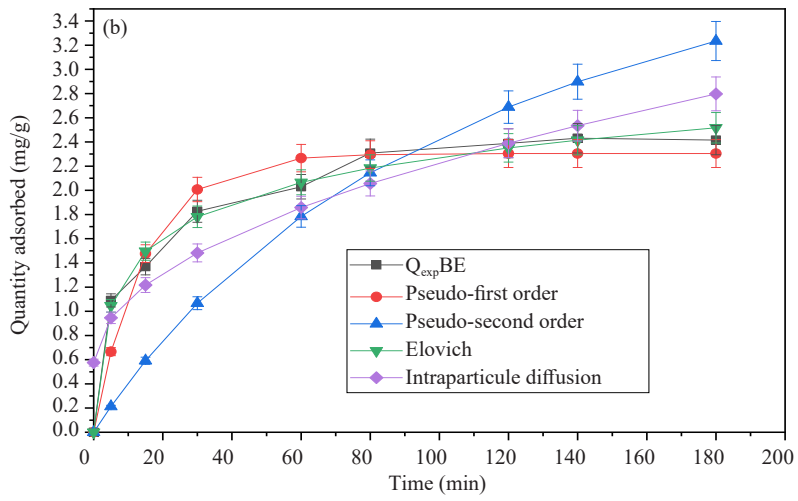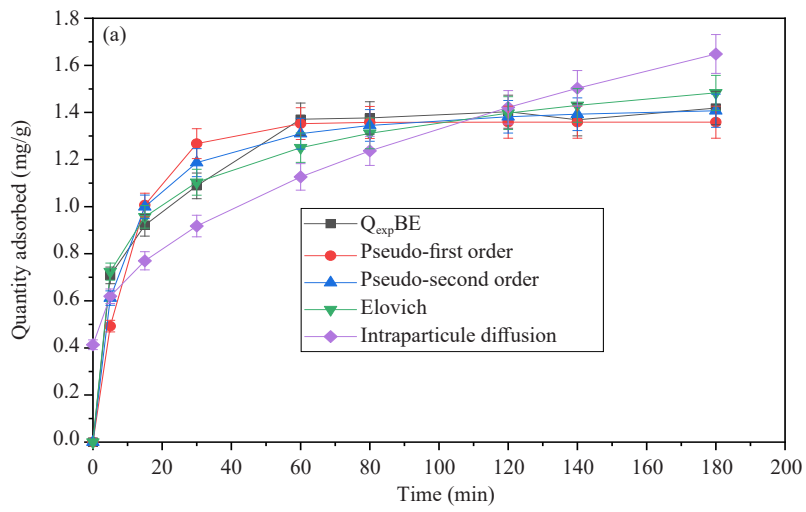
Figure 10. Non-linear forms of kinetic models for (a) BE, (b) RBE and (c) RBE@N

Table 4. Optimum kinetics parameters and their statistical comparison values onto BE, RBE and RBE@N

N°	Models	Constants	Values	R^2	χ^2	RMSE
		BE				
1.	Pseudo first-order	Q_e (mg/g)	1.359	0.952	0.132	0.304
		K_1 (1/min)	0.090			
2.	Pseudo second order	Q_e (mg/g)	1.462	0.983	0.034	0.176
		K_2 (g/min·mg)	0.099			
3.	Elovich	α (mg/g·min)	1.292	0.954	0.022	0.169
		β (g/mg)	4.721			
4.	Intraparticular diffusion	K_p (mg/g·min$^{0.5}$)	0.092	0.732	0.601	0.618
		C (mg/g)	0.413			
		RBE				
1.	Pseudo first-order	Q_e (mg/g)	2.304	0.946	0.333	0.562
		K_1 (1/min)	0.068			
2.	Pseudo second order	Q_e (mg/g)	5.447	0.978	0.100	0.345
		K_2 (g/min·mg)	0.001			
3.	Elovich	α (mg/g·min)	1.049	0.978	0.026	0.221
		β (g/mg)	2.435			
4.	Intraparticular diffusion	K_p (mg/g·min$^{0.5}$)	0.166	0.839	0.800	0.862
		C (mg/g)	0.576			
		RBE@N				
1.	Pseudo first-order	Q_e (mg/g)	2.207	0.989	0.071	0.563
		K_1 (1/min)	0.066			
2.	Pseudo second order	Q_e (mg/g)	2.420	0.928	0.044	0.370
		K_2 (g/min·mg)	0.041			
3.	Elovich	α (mg/g·min)	0.744	0.928	0.034	0.262
		β (g/mg)	2.375			
4.	Intraparticular diffusion	K_p (mg/g·min$^{0.5}$)	0.119	0.877	0.104	0.439
		C (mg/g)	0.934			

3.4 *Adsorption mechanism*

The adsorbate's nature and the adsorbent's surface characteristics are intricately linked to the adsorption mechanism. Introducing additional materials to an adsorbent modifies its surface characteristics and interactions, thereby affecting the adsorption mechanism. The most commonly identified adsorption mechanisms for clay and minerals with respect to organic water contaminants include chemical adsorption, electrostatic interaction, Van der Waals forces, hydrophobic interactions, hydrogen bonding, ion exchange, n-π interaction, surface complexation, and π-π interaction.

The dominant adsorption mode is determined by the chemical properties of the organic pollutant and the structure, surface characteristics, and functional groups of the clay mineral composites. Moreover, the adsorption mechanism is influenced by the conditions of adsorption, such as pH and ionic strength, which can alter the adsorbent's surface properties.

The typical adsorption mechanism of organic contaminants onto clay/mineral composites is depicted in Figure. 11. Three different forms of interactions may be distinguished in the case of tartrazine: dipole-dipole attractions, electrostatic attraction, hydrogen bonding, and Lewis acid-base interactions. According to Xiong et al.,[53] the Lewis interaction occurs when there is a lone pair of electrons on the adsorbent that acts as a Lewis base site to interact with the strong Lewis-acid or the adsorbate. For example, the Lewis acid (Al^{3+}) in clay or modified clay interacts with the nitrogen atom of tartrazine, which functions as a Lewis base.[54]

Although the figure does not depict the adsorption of organic contaminants, it offers valuable insights into the structure of montmorillonite, a widely utilized clay adsorbent, which is composed of octahedral and tetrahedral sheets connected by oxygen atoms.

The text accompanying the figure outlines various interactions that may occur between clay minerals and contaminants, including:

Lewis acid-base interactions: These take place between electron donors (Lewis bases) on the contaminant and electron acceptors (Lewis acids) on the clay surface.

Electrostatic attractions: The negative charge on clay surfaces can attract positively charged contaminants or repel negatively charged ones.

Hydrogen bonding: This interaction can happen between hydrogen atoms on the contaminant and oxygen atoms on the clay surface.

Ion exchange: This process involves swapping ions between the contaminant and the clay mineral.

By comprehending the interactions between contaminants and clay minerals, and how they are affected by the specific properties of each, we can more accurately predict and enhance the adsorption process to remove pollutants from water.
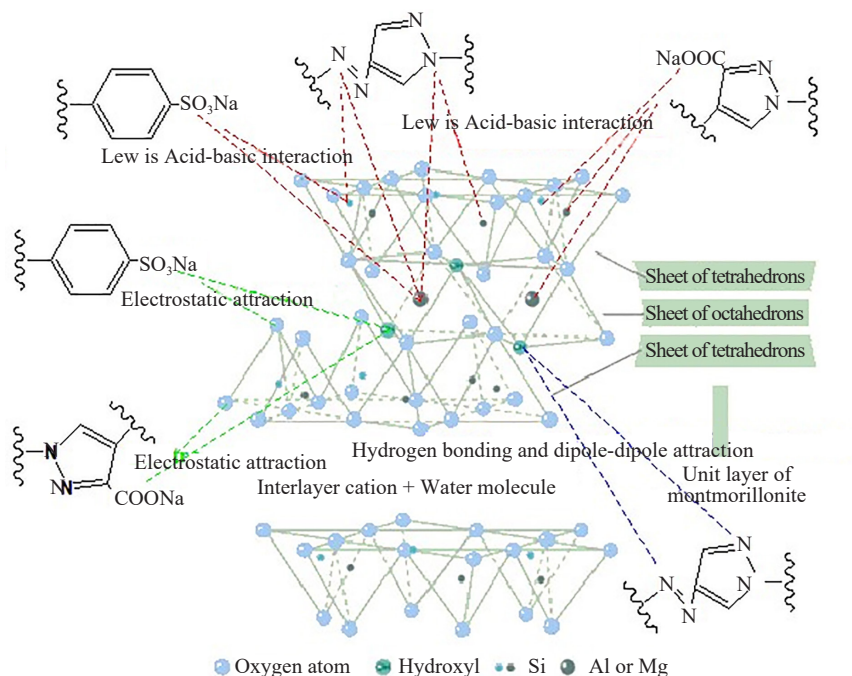
Figure 11. Proposed of adsorption mechanism of tartrazine yellow on different materials

Lewis interactions are dependent on pH since the solution's pH influences the sites that are accessible on the

adsorbent.[55] The most typical adsorption process is electrostatic contact. Electrostatic attraction and repulsion are part of the creation of ionic bonds. It is created when atoms gain and lose electrons in the presence of anions and cations. Examining how the pH of the solution affects the adsorbent's ability to adsorb is important. This is because the charges on the adsorbent might change depending on the pH of the solution, which affects the electrostatic interaction. Despite the existence of these functional groups, the electrostatic interactions through surface functional groups can occasionally be negligible.

This is a result of additional interactions present in the adsorbent, which lessen the strength of the electrostatic interactions. For example, the adsorption of malachite green onto graphene oxide/sodium montmorillonite composite was not significantly affected by electrostatic interaction.[56] A form of dipole-dipole attraction known as hydrogen bonding occurs when an electronegative atom, such as nitrogen (N), oxygen (O), or fluorine (F), bonds to a hydrogen (H) atom. The majority of clay/mineral composites have a great tendency to establish hydrogen bonds with organic pollutants.

The examination of the RBE and RBE@N materials after adsorption is depicted in Figures 12 (X-ray diffraction) and 12 (EXD/mapping). The X-ray diffraction patterns Figure 13 show that the adsorption did not change the initial material's structure, allowing for several uses and the potential for material reuse. In reference to the EDX analysis, we note that the elements on the material have changed due to the presence of carbon (C) and nitrogen (N) on the RBE diffractogram, which are elements that could only have originated from tartrazine. Additionally, it can be observed that the percentage of these elements has increased on the diffractogram of RBE@N, which originally contained these elements.
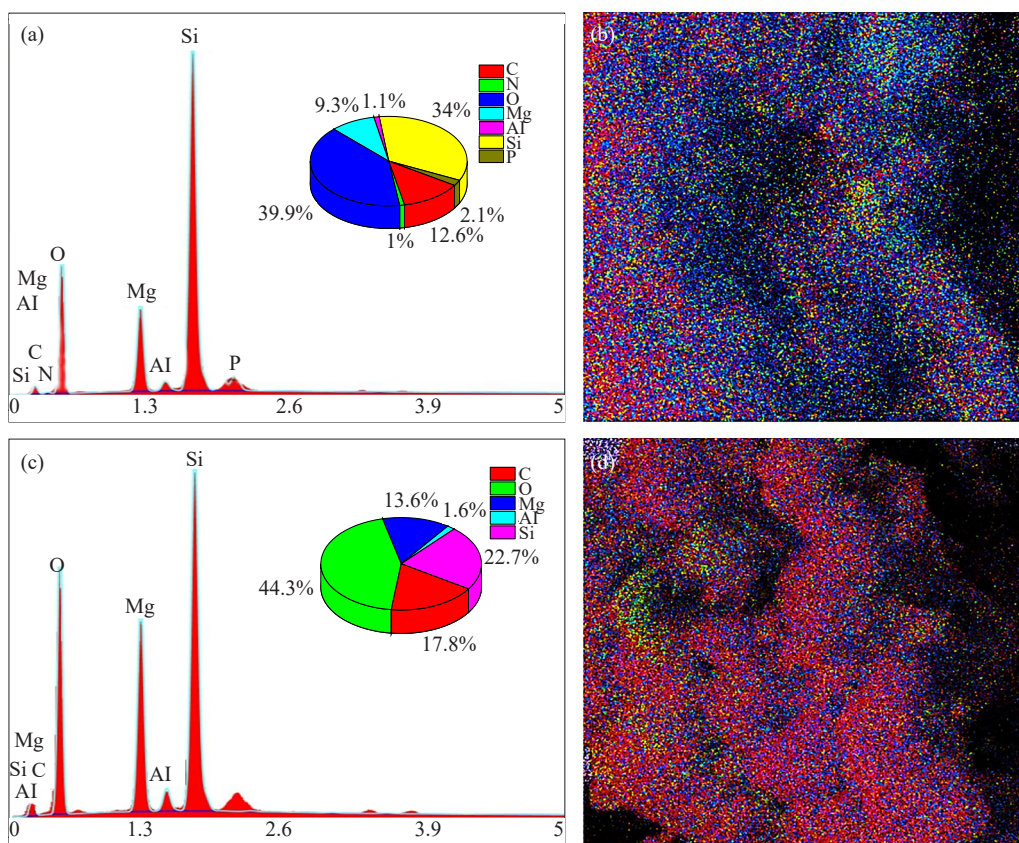
Figure 12. EDX elemental compositions (a), EDX-mapping (b) respectively for the RBE and EDX elemental compositions (c), EDX-mapping (d) element distribution mapping for the RBE@N adsorption of tartrazine
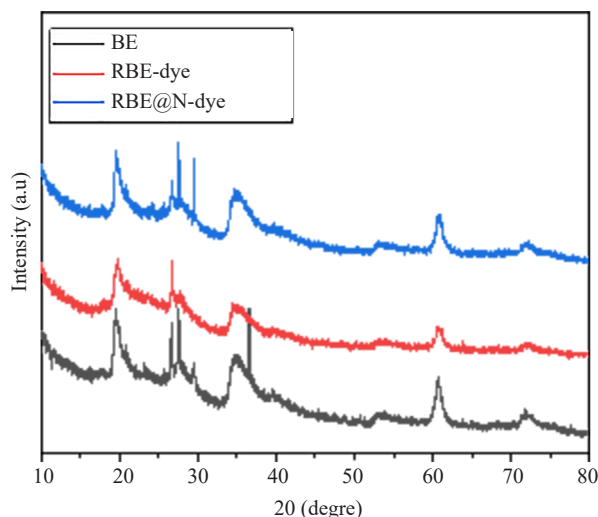
Figure 13. XRD of the materials used after E102 adsorption tests

4. Conclusion

This study investigated the removal of tartrazine yellow dye from simulated wastewater using three adsorbents: bleaching earth (BE), regenerated bleaching earth (RBE), and modified bleaching earth (RBE@N). All three effectively removed the dye, with RBE and RBE@N showing superior performance. Lower pH and lower adsorbent dosages favored dye uptake. The study also suggests that various interactions, including Lewis acid-base, dipole-dipole, hydrogen bonding, and electrostatic attraction, contribute to dye removal. The pseudo-first and pseudo-second-order kinetic models accurately represented the kinetics of dye uptake on BE, RBE, and RBE@N. The results of this study demonstrated the effectiveness of BE, RBE, and RBE@N in the decontamination of waters containing anionic tartrazine dye, with the latter two being particularly effective. There is also a competition between chemisorption and physisorption. Additionally, the analysis indicates the potential reusability of the adsorbents because they maintain their structure after dye adsorption.

Conflict of interest

The authors declare there is no conflict of interest at any point with reference to research findings.

References

[1] Tsai, W. T.; Chang, Y. M.; Lai, C. W.; Lo, C. C. Adsorption of ethyl violet dye in aqueous solution by regenerated spent bleaching earth. *J. Colloid Interface Sci.* **2005,** *289*, 333-338.

[2] Weng, C. H.; Tsai, C. Z.; Chu, S. H.; Sharma, Y. C. Adsorption characteristics of copper (II) onto spent activated clay. *Sep. Purif. Technol.* **2007,** *54*, 187-197.

[3] Talidi, A. Study on the removal of methylene blue from water using commercial activated carbon CECA40. (Engl. Transl.) *Int. J Environ. an Ch.* **2006**.

[4] Dali-Youcef, Z.; Bouabdasselem, H.; Bettahar, N. Elimination of organic compounds by local clays. *Comptes Rendus Chimie.* **2006,** *9*, 1295-1300.

[5] Tsai, W. T.; Chen, H. P.; Hsien, W. Y.; Lai, C. W.; Lee, M. S. Thermochemical regeneration of bleaching earth waste with zinc chloride. *Resources, Conservation and Recycling* **2003,** *39*, 65-77.

[6] Tsai, W. T.; Chen, H. P.; Hsieh, M. F.; Sun, H. F.; Chien, S. F. Regeneration of spent bleaching earth by pyrolysis in a rotary furnace. *J. Anal. Appl. Pyrolysis.* **2002,** *63*, 157-170.

[7] Tsai, W. T.; Lai, C. W.; Hsien, K. J. Adsorption kinetics of herbicide paraquat from aqueous solution onto

activated bleaching earth. *Chemosphere* **2004,** *55*, 829-837.

[8] Mana, M.; Ouali, M. S.; de Menorval, L. C. Removal of basic dyes from aqueous solutions with a treated spent bleaching earth. *J. Colloid Interface Sci.* **2007,** *307*, 9-16.

[9] Mahramanlıoğlu, M.; Kizilcikli, İ.; Biçer, İ. Ö.; Tunçay, M. Removal of 2, 4-D from aqueous solution by the adsorbents from spent bleaching earth. *J. Environ. Sci. Health B.* **2000,** *35*, 187-200.

[10] Al-Zahrani, A. A.; Daous, M. A. Recycling of spent bleaching clay and oil recovery. *Trans. Inst. Chem. Eng.* **2000,** *78*, 224-228.

[11] Zaviska, F. *Modeling of Organic Micro Pollutants Through Electrochemical Oxidation Treatment*; (Engl. Transl.) Canada: Institut National de la Recherche Scientifique, 2011.

[12] Chatterjee, S.; Lee, M. W.; Woo, S. H. Adsorption of congo red by chitosan hydrogel beads impregnated with carbon nanotubes. *Bioresour. Technol.* **2010,** *101*, 1800-1806.

[13] Daneshvar, N.; Rasoulifard, M. H.; Khataee, A. R.; Hosseinzadeh, F. Removal of CI Acid Orange 7 from aqueous solution by UV irradiation in the presence of ZnO nanopowder. *J. Hazard. Mater* **2007,** *143*, 95-101.

[14] Modirshahla, N.; Behnajady, M. A.; Kooshaiian, S. Investigation of the effect of different electrode connections on the removal efficiency of Tartrazine from aqueous solutions by electrocoagulation. *Dyes and Pigments* **2007,** *74,* 249-257.

[15] Tchuifon, D. R. T.; Ndifor-Angwafor, G. N.; Bopda, A.; Anagho, S. G. Modeling of phenol adsorption isotherm onto activated carbon by non-linear regression methods: Models with three and four parameters. *Desalin. Water Treat.* **2018,** *136*, 199-206.

[16] Kumar, K. V.; Porkodi, K. Batch adsorber design for different solution volume/adsorbent mass ratios using the experimental equilibrium data with fixed solution volume/adsorbent mass ratio of malachite green onto orange peel. *Dyes and Pigments* **2007,** *74*, 590-594.

[17] Subramanyam, B.; Das, A. Linearized and non-linearized isotherm models comparative study on adsorption of aqueous phenol solution in soil. *Int. J. Environ. Sci. Technol.* **2009,** *6*, 633-640.

[18] Krishni, R.; Foo, K.; Hameed, B. Adsorption of methylene blue onto papaya leaves comparison of linear and nonlinear isotherm analysis, Desalin. *Water Treat.* **2014,** *52*, 6712-6719.

[19] Kuete, I. H. T.; Tchuifon, R. D. T.; Bopda, A.; Ngakou, C. S.; Nche, G. N. A.; Anagho, S. G. Research article adsorption of indigo carmine onto chemically activated carbons derived from the cameroonian agricultural waste garcinia cola nut shells and desorption studies. *J. Chem.* **2022,** *2022*, 1236621.

[20] Grace, S.; Mafo, M.; Alain, K. N. P.; Raoul, T. T. D.; Tchuifon, T.; Fotsop, C. G.; Mve, Z.; Kenda, G. T.; Bopda, A.; Kuete, I.-H. T.; et al. Low-cost magnetic carbons-based rubber seed husks materials for highly efficient removal for reactive black 5 and reactive blue 19 textile dyes from wastewater. *J. Environ. Anal. Chem.* **2023,** *124*, 1-25.

[21] Mekuiko, A. Z.; Tchuifon, D. R. T.; Kouteu, P. A. N.; Fotsop, C. G.; Ngakou, C. S.; Tiotsop, H. I.; Bopda, A.; Tamo, A. K.; Anagho, S. G. Tailoring activated carbons based cocoa pods lignocellulosic materials for Reactive blue 19 adsorption: optimization, adsorption isotherm and kinetic investigation. *Desalin. Water Treat.* **2023,** *300*, 144-157.

[22] Alvine, L. D.; Donald R.; Tchuifon, T.; Cyrille, A. D.; Idris-Hermann, K. T.; Giscard, D.; Alain Clovis, T. D.; Anagho S. G.; Jean, N. Kinetic and isotherm studies of the adsorption phenacetin onto two copper porous coordination compounds: Nonlinear regression analysis. *J. Chem.* **2022,** *2022*, 2828860.

[23] Bopda, A.; Tchuifon, T. D. R.; Ndifor-Angwafor, N. G.; Arnaud, K. T.; Gabche, A. S. Adsorption of 2, 4-dinitrophenol on activated carbon prepared from cotton cakes: Non-linear Isotherm Modeling. *Chem. Sci. Int. J.* **2018,** *24*, 1-20.

[24] Bopda, A.; Tchuifon, D. R. T.; Nche, G. N.; Doungmo, G.; Anagho, S.G. Non-linear equilibrium and kinetic study of the adsorption of 2,4-dinitrophenol from aqueous solutionusing activated carbon derived from a olives stones and cotton cake. *Afr. J. Environ. Sci. Technol.* **2019,** *3*, 365-380.

[25] Nemgne, M. N.; Kouteu, A. P. N.; Tchuifon, D. R. T.; Ngakou, C. S.; Nche, N. A. G.; Gabche, A. S. Modeling of tartrazine dye adsorption onto treated and untreated cocoa shell by non-linear regression methods. *Modern Chem Appl.* **2022,** *10*, 383.

[26] Kuete, I. H. T.; Tchuifon, D. R. T.; Ndifor-Angwafor, G. N.; Kamdem, A. T.; Anagho, S. G. Kinetic, isotherm and thermodynamic studies of the adsorption of thymol blue onto powdered activated carbons from garcinia cola nut shells impregnated with H3PO4 and KOH: Non-linear regression analysis. *J. Encap. Adsorp. Sci.* **2020,** *10*, 1.

[27] Tchuifon, D. R. T.; Gabche, A. S.; Mbadcam, K. J.; Ndifor-Angwafor, N. G.; Nsami, N. J. Kinetics and equilibrium studies of adsorption of phenol in aqueous solution onto activated carbon prepared from rice and coffee husks. *Int. J. Eng. Sci. Technol. Res.* **2014,** *2*, 166-173.

[28] Chien, S. H.; Clayton, W. R. Application of Elovich equation to the kinetics of phosphate release and sorption in

soils. *Soil Sci. Soc. Am. J.* **1980,** *44*, 265-268.

[29] Tchuifon, T. D. R.; Anagho, S. G.; Njanja, E.; Ghogomu, J. N.; Ndifor-Angwafor, N. G.; Kamgaing, T. Equilibrium and kinetic modelling of methyl orange adsorption from aqueous solution using rice husk and egussi peeling. *Int. J. Chem. Sci.* **2014,** *12*, 741-761.

[30] El-Khaiary, M. I. Least-squares regression of adsorption equilibrium data: comparing the options. *J. Hazard. Mater.* **2008,** *158*, 73-87.

[31] Hossain, M. A.; Ngo, H. H.; Guo, W. S.; Setiadi, T. Adsorption and desorption of copper (II) ions onto garden grass. *Bioresour. Technol.* **2012,** *121*, 386-395.

[32] Djebri, N.; Boukhalfa, N.; Boutahala, M.; Chelali, N. Preparation of clay based hydrogel biomaterials, and alginate (brown algae): Environmental applications. (Engl. Transl.) *Algerian J.Environ. Sci. Technol.* **2017,** *3*, 532-538.

[33] Er-ramly, A.; Ider, A. Physico-chemical and mineralogical characterization of a Moroccan bentonite (Azzouzet) and determination of its nature and its chemical structure. *Int. J.Material. Sci. Appl.* **2014,** *3*, 42-48.

[34] Qlihaa, A.; Dhimni, S.; Melrhaka, F.; Hajjaji, N.; Srhiri, A. Physical and chemical properties of clay moroccan [Physical-chemical characterization of a morrocan clay]. (Engl. Transl.) *J. Mater. Environ. Sci.* **2016,** *7*, 1741-1750.

[35] Akdim, M.; Mesrar, L.; Boukili, B.; Jabrane, R. Physicochemical characterization of mixtures of the Miocene marl of Fez vicinity, cellulose and pozzolan. *J. Mater. Environ. Sci.* **2017,** *8*, 2747-2756.

[36] Abid, W.; Mahmoud, I. B.; Masmoudi, S.; Triki, M. A.; Mounier, S.; Ammar, E. Physical-chemical and spectroscopic quality assessment of compost from date palm (Phoenix dactylifera L.) waste valorization. *J. Environ. Manage.* **2020,** *264*, 110492.

[37] Lian, L.; Guo, L.; Guo, C. Adsorption of Congo red from aqueous solutions onto Ca-bentonite. *J. Hazardous Material.* **2009,** *161*, 126-131.

[38] Batana, F. Z.; Taouti, M. B.; Guibadj, A. The adsorption kinetics of methylene blue on crude bentonite, and treatment. (Engl. Transl.) *Algerian J. Environ. Sci. Technol.* **2019,** *5*, 1113-1120.

[39] Komadel, P.; Madejová, J.; Stucki, J. W. Structural Fe (III) reduction in smectites. *Appl. Clay Sci.* **2006,** *34*, 88-94.

[40] Fernandes, C.; Catrinescu, C.; Castilho, P.; Russo, P. A.; Carrott, M. R.; Breen, C. Catalytic conversion of limonene over acid activated Serra de Dentro (SD) bentonite. *Appl. Catalysis A: General.* **2007,** *318*, 108-120.

[41] Belmoujahid, Y.; Bonne, M.; Scudeller, Y.; Schleich, D.; Grohens, Y.; Lebeau, B. Thermal conductivity of monolithic assemblies of SBA-15 ordered mesoporous silica particles. *Microporous and Mesoporous Materials.* **2015,** *201*, 124-133.

[42] Zaghouane-Boudiaf, H.; Boutahala, M. Kinetic analysis of 2, 4, 5-trichlorophenol adsorption onto acid-activated montmorillonite from aqueous solution. *Int. J. Mineral. Process.* **2011,** *100*, 72-78.

[43] Özcan, A. S.; Erdem, B.; Özcan, A. Adsorption of Acid Blue 193 from aqueous solutions onto Na-bentonite and DTMA-bentonite. *J. Colloid Interface Sci.* **2004,** *280*, 44-54.

[44] Banerjee, S.; Chattopadhyaya, M. C. Adsorption characteristics for the removal of a toxic dye, tartrazine from aqueous solutions by a low cost agricultural by-product. *Arab. J. Chem.* **2017,** *10*, S1629-S1638.

[45] Gupta, V. K.; Jain, R.; Shrivastava, M.; Nayak, A. Equilibrium and thermodynamic studies on the adsorption of the dye tartrazine onto waste "coconut husks" carbon and activated carbon. *Journal of Chemical & Engineering Data.* **2010,** *55*, 5083-5090.

[46] Mohammed, A. A.; Al-Musawi, T. J.; Kareem, S. L.; Zarrabi, M.; Al-Ma'abreh, A. M. Simultaneous adsorption of tetracycline, amoxicillin, and ciprofloxacin by pistachio shell powder coated with zinc oxide nanoparticles. *Arab. J. Chem.* **2020,** *13*, 4629-4643.

[47] Ezekoye, O. M.; Akpomie, K. G.; Eze, S. I.; Chukwujindu, C. N.; Ani, J. U.; Ujam, O. T. Biosorptive interaction of alkaline modified Dialium guineense seed powders with ciprofloxacin in contaminated solution: Central composite, kinetics, isotherm, thermodynamics, and desorption. *Int. J. Phytoremediation.* **2020,** *22*, 1028-1037.

[48] Ndifor-Angwafor, N. G.; Tiotsop, I. K.; Tchuifon, D. T.; Ngakou, C. Biosorption of amaranth red in aqueous solution onto treated and untreated lignocellulosic materials (pineapple peelings and coconut shells). *J. Mater. Environ. Sci.* **2017,** *8*, 4199-4212.

[49] Anagho, S. G.; Ketcha, J. M.; Tchuifon, T. D. R.; Ndi, J. N. Kinetic and equilibrium studies of the adsorption of mercury (II) ions from aqueous solution using kaolinite and metakaolinite clays from Southern Cameroon. *Int. J. Res. Chem. Environ.* **2013,** *3*, 1-11.

[50] Tchuifon T. D. R.; Ndifor-Angwafor, N. G.; Christian, N. S.; Théophile, K.; Manga, N. H.; Gabche, A. S.; Mbadcam, K. J. Optimization of cadmium (II) adsorption onto modified and unmodified lignocellulosics (rice husk

and egussi peeling). *Int. J.Basic Appl. Sci.* **2016,** *5*, 45.

[51] Das, B.; Mondal, N. K. Calcareous soil as a new adsorbent to remove lead from aqueous solution: Equilibrium, kinetic and thermodynamic study. *Univers. J. Environ. Res. Technol.* **2011,** *1*, 515-530.

[52] Yadav, S. K.; Singh, D. K.; Sinha, S. Chemical carbonization of papaya seed originated charcoals for sorption of Pb (II) from aqueous solution. *J. Environ. Chem. Eng.* **2014,** *2*, 9-19.

[53] Xiong, D. G.; Zhang, Z.; Huang, X. Y.; Huang, Y.; Yu, J.; Cai, J. X.; Yang, Z. Y. Boosting the polysulfide confinement in B/N-codoped hierarchically porous carbon nanosheets via Lewis acid-base interaction for stable Li-S batteries. *J. Energy Chem.* **2020,** *51*, 90-100.

[54] Ouachtak, H.; El Haouti, R.; El Guerdaoui, A.; Haounati, R.; Amaterz, E.; Addi, A. A.; Taha, M. L. Experimental and molecular dynamics simulation study on the adsorption of Rhodamine B dye on magnetic montmorillonite composite γ-Fe$_2$O$_3$@ Mt. *J. Mol. Liq.* **2020,** *309*, 113142.

[55] Liu, S.; Liu, Y.; Jiang, L.; Zeng, G.; Li, Y.; Zeng, Z.; Ning, Q. Removal of 17 *β*-Estradiol from water by adsorption onto montmorillonite-carbon hybrids derived from pyrolysis carbonization of carboxymethyl cellulose. *J. Environ. Manage.* **2019,** *236*, 25-33.

[56] Arabkhani, P.; Asfaram, A.; Ateia, M. Easy-to-prepare graphene oxide/sodium montmorillonite polymer nanocomposite with enhanced adsorption performance. *J. Water Process Eng.* **2020,** *38*, 101651.